J Seismol (2009) 13:543–559
DOI 10.1007/s10950-008-9145-8

ORIGINAL ARTICLE

Inversion of Scholte wave dispersion and waveform modeling for shallow structure of the Ninetyeast Ridge

Xuan Nhi Nguyen · Torsten Dahm · Ingo Grevemeyer

Received: 26 March 2007 / Accepted: 10 November 2008 / Published online: 19 December 2008

Abstract The construction of S-wave velocity models of marine sediments down to hundreds of meters below the seafloor is important in a number of disciplines. One of the most significant trends in marine geophysics is to use interface waves to estimate shallow shear velocities which play an important role in determining the shallow crustal structure. In marine settings, the waves trapped near the fluid–solid interface are called Scholte waves, and this is the subject of the study. In 1998, there were experiments on the Ninetyeast Ridge (Central Indian Ocean) to study the shallow seismic structure at the drilled site. The data were acquired by both ocean bottom seismometer and ocean bottom hydrophone. A new type of seafloor implosion sources has been used in this experiment, which successfully excited fast and high frequency (>500 Hz) body waves and slow, intermediate frequency (<20 Hz) Scholte waves. The fundamental and first higher mode Scholte waves have both been excited by the implosion source. Here, the Scholte waves are investigated with a full waveform modeling and a group velocity inversion approach. Shear wave velocities for the uppermost layers of the region are inferred and results from the different methods are compared. We find that the full waveform modeling is important to understand the intrinsic attenuation of the Scholte waves between 1 and 20 Hz. The modeling shows that the S-wave velocity varies from 195 to 350 m/s in the first 16 m of the uppermost layer. Depths levels of high S-wave impedance contrasts compare well to the layer depth derived from a P-wave analysis as well as from drilling data. As expected, the P- to S-wave velocity ratio is very high in the uppermost 16 m of the seafloor and the Poisson ratio is nearly 0.5. Depth levels of high S-wave impedance contrasts are comparable to the layer depth derived from drilling data.

Keywords Scholte wave · Sediments · Seismic waves · Shear deformation · Velocity measurement · Seafloor phenomena · Waveform modeling · Dispersion (waves) · Sensitivity kernel · Implosive source

X. N. Nguyen (✉) · T. Dahm
Institut für Geophysik, Universität Hamburg,
Bundesstrasse 55, 20146 Hamburg, Germany
e-mail: nhi.nguyen@zmaw.de

X. N. Nguyen
Institut für Geophysik,
Technische Universität Bergakademie Freiberg,
Gustav-Zeuner-Straße 12, 09599 Freiberg, Germany

I. Grevemeyer
IFM–GEOMAR,
Leibniz Institut für Marine Geowissenschaften,
Wischhofstrasse 1-3, 24148 Kiel, Germany

1 Introduction

The S-wave velocities structure of marine sediments beneath the seafloor has many practical applications. In seismic exploration, these models would help to improve the S-wave static correction needed in oil and gas exploration. Images of deep horizons derived from S-waves are sometimes better than those achievable from P waves and additionally provide estimates of Poisson's ratio which is used as a proxy for porosity. Information of sedimentary acoustic properties is needed to understand acoustic wave loss, which is important for sonar propagation, particularly in shallow water.

The knowledge of parameters of the mushy layer (soft marine sediment) has other important applications. For instance, S-wave incidence angles are steepened to sub-vertical directions and arrivals are systematically retarded by a few fractions of a second. Knowledge of the systematic time shift is of relevance for local earthquake studies and seismic tomography. Due to the strong impedance contrast for S-waves in the uppermost soft layers, incoming P waves generate strong P-to-S converted phases arriving slightly later than the P wave and often causing monochromatic ringing on both horizontal and vertical components of seismometers. The dominant frequency and the relative arrival of the converted phase can be predicted when knowing parameters of the mushy layer (e.g., Thorwart 2006). The P- and S-wave velocities are also required when decomposing the wavefield in up- and down-going waves. Wave-field decomposition techniques have been successful to suppress water layer multiples in active seismic (e.g., Amundsen and Reitan 1995; Osen et al. 1999) or passive seismology studies (e.g., Thorwart and Dahm 2005). The shear strength of the mushy layer is quite small. This is of relevance when studying the shear stability of uppermost soft layers for an inclined sea bottom.

To obtain the in situ S-wave velocity structure of shallow-water marine sediments, we analyze dispersive interface waves traveling along the interface between water and sediments, the so-called Scholte waves.

Scholte waves have a particle motion similar to that of the Rayleigh wave, but its propagation velocity is slightly lower because of its interaction with the overlying water. In the low frequency or long-wavelength limit, the water layer can be neglected and the Scholte waves can be regarded as Rayleigh waves (Bohlen et al. 2004). For higher frequencies, it is a modified version of the Rayleigh wave that is trapped by the water–sediment interface. Sediment layering, as well as the finite water depth, disperses the Scholte wave. Phase and group velocities of Scholte waves between 1 and 20 Hz are primarily sensitive to S-wave velocity of the uppermost few tens of meters of the sediment floor. Since the geometrical spreading of interface waves is smaller than the one of high frequency body waves, higher Scholte wave amplitudes and longer traveling path can be generally expected for Scholte waves.

The prerequisite to the efficient generation of dispersed interface waves (Scholte waves) is that the location of the source should be at the seafloor or very close to the seafloor. Additionally, the recording seismometer should be sensitive at low frequency (wide-band sensors).

Recently, there have been a number of advanced studies about Scholte waves in ocean sediment layers. Nolet and Dorman (1996) adapted method of non-linear waveform fitting to accommodate multidimensional model and applied it to invert several record sections of Scholte waves. Ritzwoller and Levshin (2002) presented multi-wave inversion method which can adapt to a wide variety of information in marine seismic data. Forbriger (2003a, b) described his new approach on the inversion of shallow-seismic wavefields. The first stage of this full wavefield inversion is to calculate the transform of a complete representation of data by using a discrete approximation to the Bessel transformation. In the second stage, 1-D model of the subsurface from the transform and P-wave arrival times are inferred by fitting them with their synthetic counterpart. Recently, Bohlen et al. (2004) inferred 2-D shear wave velocity structure of shallow-water marine sediments from the lateral variation of Scholte wave dispersion. Scholte wave was recorded also by

OBS and excited by air gun. An offset of window was used to move along the common receiver gather to pick up a local wavefield. Corresponding to each local wavefield, the shear wave velocity depth profile was obtained. As the window continuously moves along the common receiver gather, a 2-D S-wave velocity section was generated.

Here, we analyze data from an experiment in 1998 on the Ninetyeast Ridge (Central Indian Ocean) to study the shallow seismic structure at the drilled site. The data were acquired by both ocean bottom seismometer (OBS) and ocean bottom hydrophones (OBH). The implosive sources were at distances of 813 to 2,096 m from the receivers.

The body wave analysis of Grevemeyer et al. (1999) showed a good agreement between the P-wave seismic structure and the results obtained by drilling. The shear wave seismic structure has not been analyzed with the data so far and is studied in this paper. Actually, the S-wave velocity of marine sediments has been difficult to measure. The Scholte wave analysis provides an independent approach. The paper is aimed as a principal investigation of Scholte wave analysis at 1–20 Hz from the new type of implosive seismic source and 1 Hz ocean bottom seismometer. It is organized as follows: first, we briefly describe the experiment setup. After that, the main characteristics of the implosive source are discussed. The following chapters describe the dispersion analysis, inversion, and waveform modeling to infer the S-wave velocity of the uppermost 150 m. The paper concludes with a brief comparison and discussion.

2 Experiment setup

In 1988, the Ninetyeast Ridge was chosen by the international scientific community for the installation of the first seismic International Ocean Network station, known as NERO (Ninetyeast Ridge Observatory). The main objective of the cruise (named SO 131) was to investigate the local and regional crustal structure around NERO. So far, several reports about the analysis of the experimental data were published.

Ninetyeast Ridge, a major seismic ridge in the Indian Ocean, can be traced for about 5,000 km from 30°S northward into the Bay of Bengal, where it is buried beneath the Bengal fan. Paleomagnetic, bathymetric, and geochemical data all support the idea that Ninetyeast Ridge formed in Late Cretaceous to Early Eocene times above a mantle plume now located beneath the Kerguelen archipelago (Peirce et al. 1989a).

Sites 757 (or 1107) are on the eastern edge of the summit horst near 17°S, downdip to the southeast from the structural crest. Three lithological units have been cored (Peirce et al. 1989a). Unit I is composed of Pleistocene to Lower Eocene nanofossil ooze; unit II is composed of volcanic ashes and tuffs; unit III provided basaltic flows with some evidence of intercalated ash material.

A location about 5 km to the south of sites 757 and 1107 provided a flat seabed with horizontally layered strata (Flueh and Reichert 1998). Two pairs of OBS or OBH were placed along a west–east trending line. A 2-km line of five bottom implosion sources were placed between the OBS/OBH pair and measurements on one OBS (OBS88, LE1D 1 Hz sensor, see Fig. 1) are usable for our analysis. The implosion sources are called

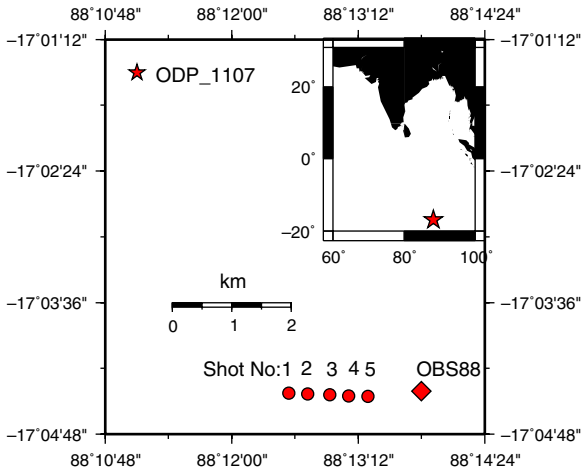

Fig. 1 Location map showing the layout of the experiment. *Diamond* is ocean bottom receiver OBS88; *circles* are bottom implosion sources (shots no. 1–5)

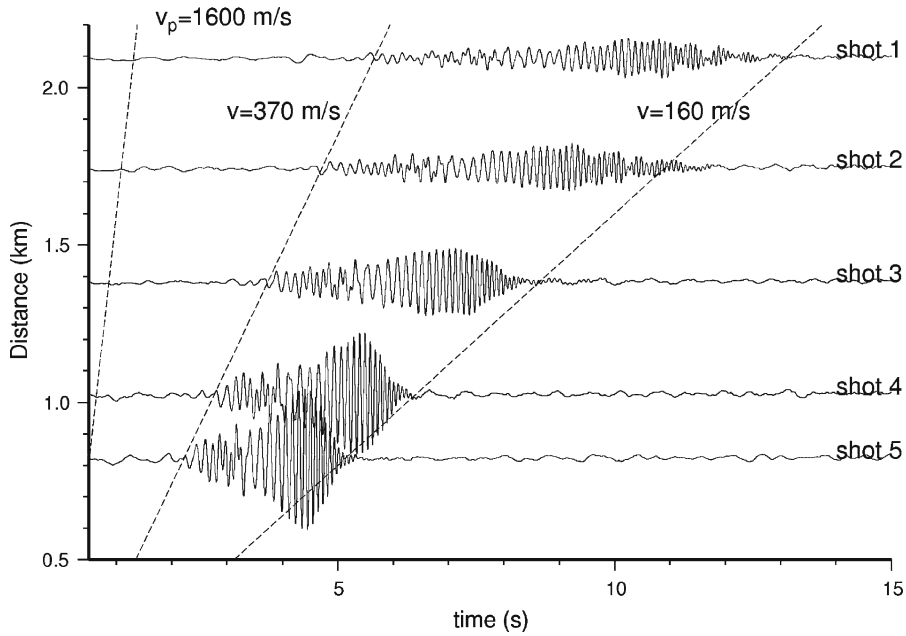

Fig. 2 Record section of vertical component seismograms from the five seafloor shots observed at OBS88. Data (*solid line*) are unfiltered but integrated (1,000 Hz sampling rate) and amplitudes are scaled to a common factor. The *dashed lines* indicate approximate propagation velocities of direct P waves (1,600 m/s) and Scholte waves (between 370 and 160 m/s)

"shot" in the following. The source location is estimated by a relocation procedure using direct water waves and the whole station network (Herber et al. 1999). The location accuracy is in between ±15 m and the shooting times are estimated within about milliseconds. All five shots have identical moment and radiation patterns.

Figure 2 shows vertical component seismograms recorded at OBS88 from shots 5–1 in distances between 813 and 2,096 m. The onset of the direct P waves is hardly seen in Fig. 2, but it looks much clearer if hydrophone data (4,000 Hz sampling rate) are shown. The largest amplitudes on the seismograms arrive later than the body waves and represent the arrival of the Scholte waves. The energy transported by Scholte modes decreases with station–shot distance and the duration of the wave trains increases with distance due to strong velocity dispersion. The seismograms are regularly dispersive, i.e., lower frequency wave groups arrive earlier than the higher frequency groups, and limiting group velocities are between 160 and 370 m/s. Two wave groups with higher amplitudes can be recognized. The strongest one occurs at the tail of the dispersive wave train and may be associated with an Airy-type phase caused by the limiting group velocity of the upper layer. The second group is much smaller and arrives earlier than the arrival of the Scholte wave fundamental mode. As discussed below, this group is interpreted as the first higher mode.

3 Characteristics of the implosive source

A technical description of the implosive source and its P-wave generation are given in Herber et al. (1999). Here, we concentrate on the aspects of Scholte wave generation. The implosive source itself is a 25.4 cm diameter (10 in.) BENTHOS hollow glass sphere with a small hole in the wall for an electrical connector using underwater plugs. In the sphere, a small explosive charge (two electrical detonators, about 1 g of explosives) is fixed on the 0.9-cm-thick glass wall. The time of detonation of explosives is controlled by an external shooting device with a clock, where drift due to temperature change is measured and corrected during processing. After detonation, the glass wall is destabilized and the ambient water pressure causes the implosion.

The radiation pattern for Scholte waves is isotropic, i.e., the implosive source radiates Scholte waves with same amplitudes and phase in all azimuth directions. For numerical modeling studies, the implosion can be simulated by

an explosive source where the source wavelet is multiplied by −1.

The low frequency strength of the implosion source is defined by the seismic moment of an isotropic source (Müller 2001): $M_I = (\lambda + 2\mu)\,\Delta V \approx \lambda \Delta V$

With the use of ideal gas equation $PV = P_0 V_0$, we obtain: $\Delta V = V_0 \left(\frac{P_0}{P_0 + \rho g z} - 1 \right)$, where:

ΔV, P_0, V_0	volume difference, atmospheric pressure, and initial volume of the source
μ, λ	shear modulus, Lame modulus, for water, $\mu = 0$, $\lambda \approx 2.25 \cdot 10^9$ N/m^2
ρ, z	density of water, depth of the source

The seismic moment of the implosion source is shown in Fig. 4.

The time scale of the implosion process and the possible bubble oscillation of the compressed air are not well known. The initial implosion is most likely fast and can be associated with the radiation of high frequency waves up to 1,000 Hz as observed on hydrophones during the experiment (see Herber et al. 1999). The dominant frequencies of possible air bubble oscillations may be much smaller. Following empirical formulas for the period of air-gun bubble oscillations (e.g., Parkes and Hatton 1986), we would estimate a dominant frequency of our 10-in. sphere in the range of 7 Hz. Figure 3 shows an amplitude spectrum of the Scholte wave train at OBS 88 from the nearest shot. Most energy is distributed below 15 Hz. The spectrum is not flat but shaped with largest amplitudes between 7 and 11 Hz. Equidistant peaks ride on the Gaussian-shaped spectrum and indicate a possible low frequency resonance effect of unknown origin. The curved spectral shape of the signal is clearly different in comparison with signals from earthquakes and may influence the group velocity estimates.

It has been disputed over what parameters control the strength of implosive sources at frequencies below 200 Hz and to what distance Scholte and other waves excited by implosion sources may be recorded at the seafloor. The seismic moment increases over the first 100 m water depth and is nearly constant at deeper levels. At this depth, the moment, or the equivalent magnitude, is linearly related to the implosive volume (Fig. 4). A 10-in. sphere (12.7 cm radius) would lead to an equivalent magnitude of $M = -1.2$ at $z > 200$ m

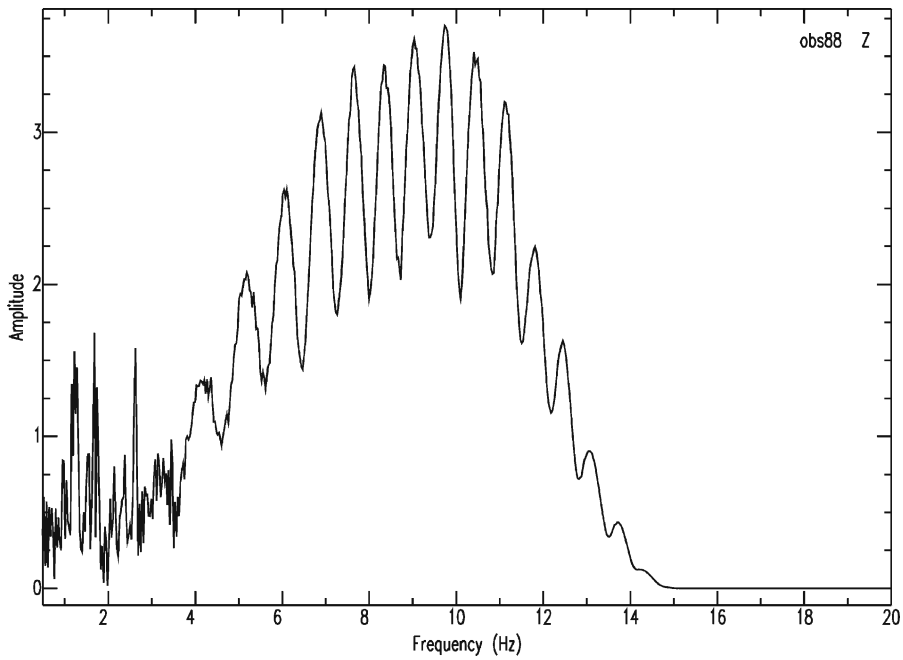

Fig. 3 Amplitude spectrum of the seismogram from shot 5. Data have been mean removed, tapered, and integrated. Sampling rate was 4,000 Hz and the sensor corner frequency is at 1 Hz

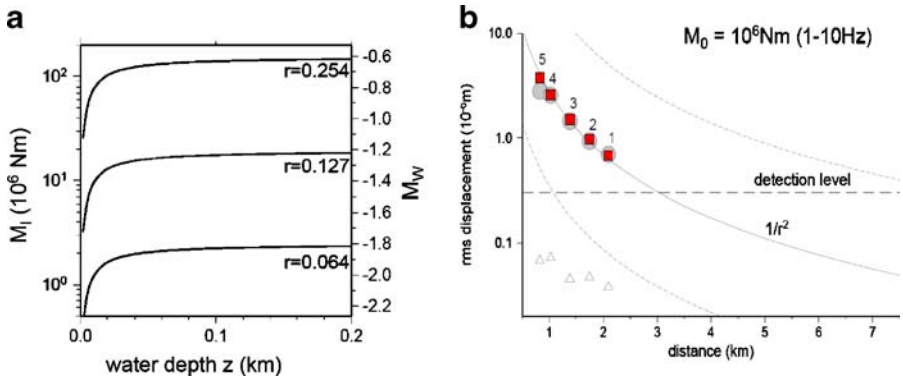

Fig. 4 **a** Seismic moment M_I and moment magnitude M_W of the implosion source as a function of depth. The 10-in. benthos sphere used in this study had a radius of a = 12.7 cm. Predicted moments of the sphere with double and half this radius is plotted for comparison. **b** Amplitude attenuation curve of Scholte waves between 1 and 13 Hz and for a moment of 10^6 Nm. *Gray-filled circles* give the rms amplitudes of the observed seismogram and *red squares* the amplitudes retrieved from synthetic full waveforms that considered strong intrinsic attenuation of Q = 40. The *continuous and dashed lines* give a $1 / r^2$ attenuation relation. Note that the attenuation of synthetic Airy-phase waveforms would be smaller in the range of $1 / r$ to $1 / r^2$ if intrinsic attenuation would be absent. The *triangles* are the rms amplitude from the time window before the onset of Scholte waves (noise level plus body wave energy). The *numbers* indicate shots. The detection level is as much as six times higher than the amplitude of the ambient noise

(Fig. 4) Using a sphere of a doubled diameter gives eight times higher moment or a moment magnitude of $M_W = -0.75$. The same source strength may be reached if 8- to 10-in. spheres are fired simultaneously. The expected distance range to where 1–15 Hz Scholte waves can be analyzed depends on different parameters such as the seafloor background noise, the depth and strength of S-wave impedances in the uppermost layers, and the intrinsic attenuation. In Fig. 4b, we plot the amplitude attenuation curve of the Scholte waves measured in our experiment, together with an estimate of noise. Root mean square (rms) amplitudes attenuate approximately with $1 / r^2$, which is larger than the expected square root attenuation of surface waves. The comparison with synthetic seismograms indicates that such a strong amplitude attenuation can be explained by high intrinsic attenuation in the range of Q = 40. This will be further discussed in Section 5. The approximate detection distance in Fig. 4b is estimated from the crossing point of the extrapolated attenuation curve with a level six times higher than the noise amplitude. The 10-in. source has a detection distance of about 3 km only. A source of doubled radius has an expected Scholte wave detection level of slightly more than 7.5 km.

4 Data analysis

We will discuss the data processing of observational data to provide group velocity U and phase velocity c, velocity dispersion curves which can be used for inversion to infer S-wave velocity profile. The section addresses methods for determination of group velocity and phase velocity.

4.1 Group velocity analysis

The data recorded at the OBS station are analyzed by calculating the group velocity of different frequency components of the Scholte waves using the travel time and the total distance from the source to receiver. A multiple filter technique (MFT; see Dziewonski et al. 1969 and Bhattacharya 1983) is applied to estimate the frequency-dependent group velocity. So-called Gabor diagrams have been calculated and analyzed. In this process, each trace is transformed into the frequency domain

and narrow-band filtered at a series of different center frequencies. A Gaussian filter is applied with a relative bandwidth of 0.12 (equivalent to $\alpha = 208$, see Dziewonski et al. 1969). For each center frequency, the instantaneous amplitude and frequency are calculated signal envelopes and are griddled and plotted (Fig. 5a).

A non-flat spectral shape of the source may influence the estimate of group velocities. Therefore, it is important to use a Gaussian filter with small bandwidth to obtain unbiased estimates. On the other hand, a narrow bandwidth of the filter in the frequency domain leads to broad and long signals in the time domain. Higher modes with arrival times close to the fundamental mode are possibly hidden in the filtered signal of fundamental mode. Such a case is observed in Fig. 5a for the closest shot. At a center frequency of 4.8 Hz, the first higher mode signal is hidden in the broadened signal of the stronger fundamental mode if a bandwidth of 0.12 is used. To avoid this problem we apply a phase-matched filter (PMF; Herrin and Goforth 1977) in order to separate the fundamental and first higher mode before filtering. An iterative technique is used to find a phase-matched filter for each particular shot–station distance.

We first apply MFT using a relatively broad bandwidth to identify fundamental and higher modes and to get a first estimate of the fundamental mode group velocity (Fig. 5a). The group velocities have to be independently confirmed by plotting sections of band-pass-filtered seismograms. The PMF is then defined to separate fundamental and first higher mode. The Gabor matrix is built for both separated signals and applied to a narrow bandwidth with high frequency resolution. The MFT and PMF techniques are iteratively applied to improve the estimates. The process is illustrated for the closest and farthest shot in Fig. 5c and d. The separated time domain record sections are plotted in Fig. 6 and nicely illustrate the effect of mode separation

It may be noted that group velocities in Fig. 6 appear to vary systematic with distance. The closest shot show smaller and more distant shot faster velocities compared to the average. The reason is unknown to us but we speculate that the strong intrinsic attenuation may influence the estimates because higher frequencies are more and more attenuated with increasing distance. However, the variation of group velocities between different shots is small. The results show that the group velocity of the fundamental mode travels between 160 and 170 m/s at high frequencies of 16 Hz to 300 m/s at 3 Hz. The first higher mode has a group velocity of 400 m/s at 3 Hz which slows down to 260 m/s at frequencies of 16 Hz.

The dispersion curves of the fundamental mode are more reliable between 4 and 16 Hz where most signal energy is excited.

We further observed a systematic shift of group velocities to higher values when increasing the bandwidth of the Gaussian filter. The possible influence of the filter bandwidth is well known and is predicted to be larger if the source spectrum is curved as in our case (e.g., Herrmann and Ammon 2004). For the final interpretation, we therefore use corrected estimates of group velocities as described by Herrmann and Ammon (2004).

4.2 Phase velocity determination

The isolated fundamental mode Scholte waves from different shots have additionally been used to determine phase velocity dispersion curves. In the study, the Fourier transform of the slant stack from all five shots is plotted for varying phase velocities (slowness). Maxima of the stacks in frequency–velocity space have been analyzed and associated with the phase velocity curve of the mode. The slant stack method is described in detail in McMechan and Yedlin (1981) and implemented in the method of Herrmann and Ammon (2004) (program SURF96).

Unfortunately, the slant stacks are difficult to interpret because of strong aliasing effects resulting from the large shot distances. Strong side lobes are present and make an unambiguous and correct picking of the fundamental mode phase velocity difficult, especially at high frequencies. We therefore restrict the picking to low frequencies between 3 and 5 Hz, where relatively strong and clear maxima are found.

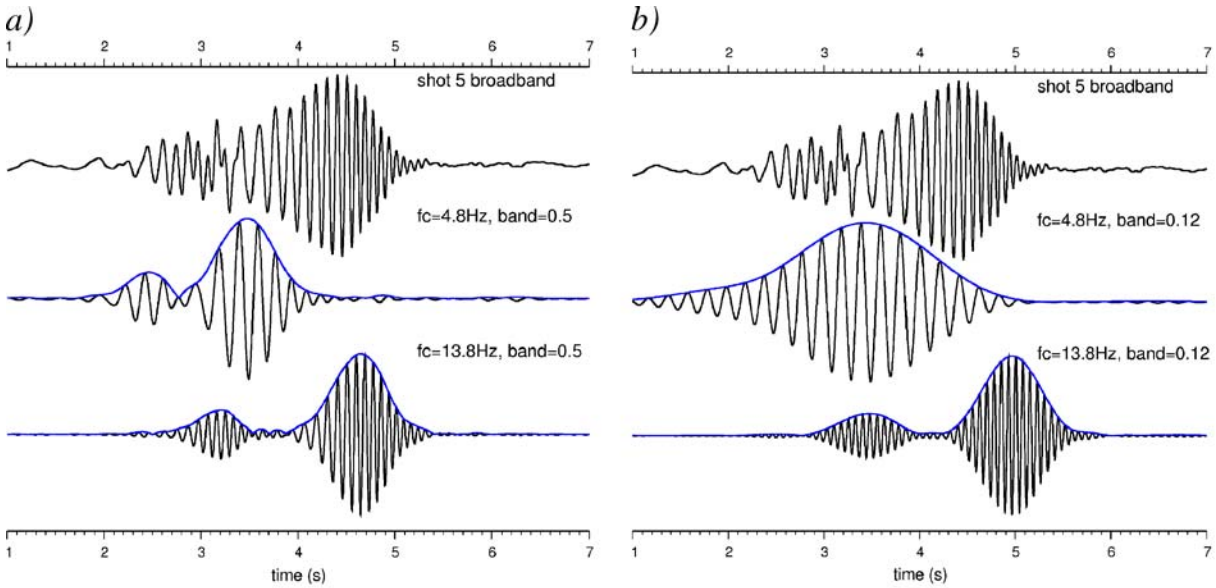
a)
shot 5 broadband
fc=4.8Hz, band=0.5
fc=13.8Hz, band=0.5
time (s)
b)
shot 5 broadband
fc=4.8Hz, band=0.12
fc=13.8Hz, band=0.12
time (s)

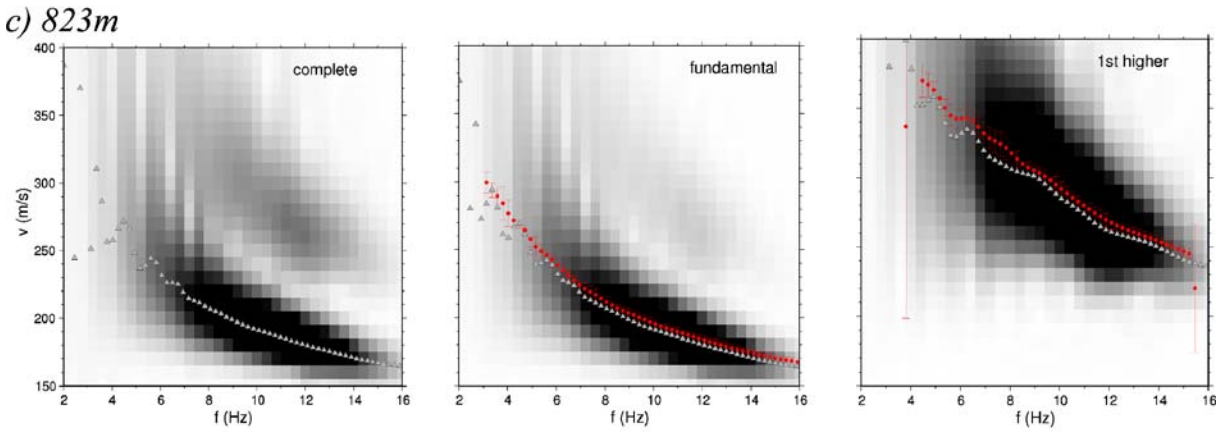
c) 823m
complete
fundamental
1st higher
v (m/s)
f (Hz)

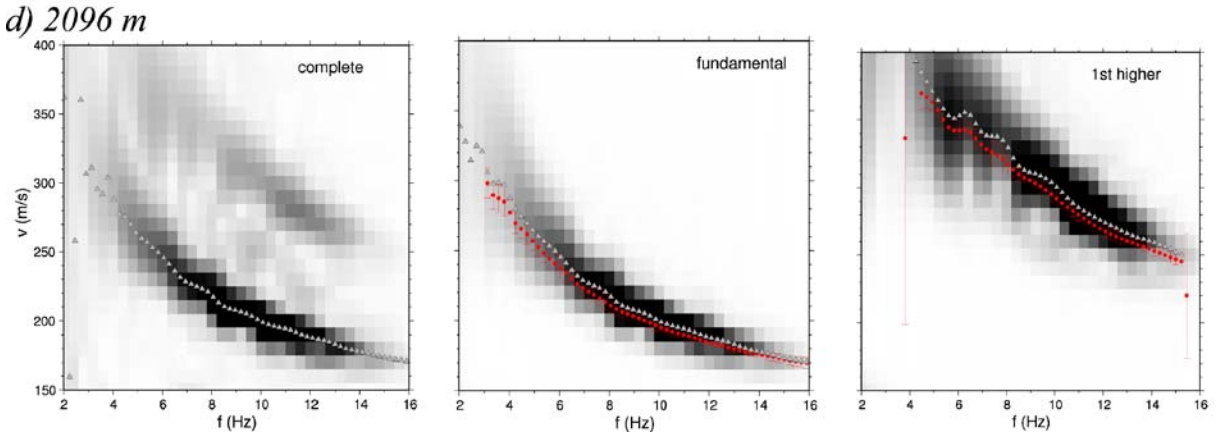
d) 2096 m
complete
fundamental
1st higher
v (m/s)
f (Hz)

◀ **Fig. 5** **a** Broadband seismogram for shot 5 (*top*) and filtered signals and envelopes for center frequencies at 4.8 and 13.8 Hz and a bandwidth of 0.5. **b** The same as in (**a**) but for a narrow bandwidth of 0.12. **c** (823 m), **d** (2,096 m) Gabor matrices of the original (*left*) and separated fundamental (*middle*) and higher mode signal (*right*). The closest (no. 5) and farthest shot (no. 1) are shown in (**c**) and (**d**), respectively. Envelope amplitudes have been scaled to their maximum and griddled by the GMT software. Absolute maxima of envelopes (*triangles*) have been automatically picked and *error bars* represent standard deviations from all five shots

Figure 7 shows all estimated dispersion curves, i.e., group velocities u_0 (fundamental mode) and u_1 (first higher mode) between 3.5 and 15 Hz and the fundamental mode phase velocity between 3 and 5 Hz. The correct picking of the short branch of phase velocities is confirmed by the comparison of the associated (derived) group velocities with the direct measurements in the overlapping frequency range (Fig. 7).

5 Inversion for shear wave velocity

In this section, we would like to present some of our inversion results. We actually used direct search algorithm (Wathelet et al. 2004) and damped linear inversion (Herrmann and Ammon 2004) to infer shear wave velocity. The second scheme seems to be more dependent on starting models. In the following, we present the inversion results obtained by direct search algorithm.

Parametric studies indicate that the S-wave velocity and the thickness of the layers are the parameters to which the wave dispersion is more sensitive, while the mass density and P-wave velocity have smaller ranges of influence. It is further known that the P- to S-wave velocity ratio within the unconsolidated sediments which are usually encountered near the seafloor (mushy layer) is generally greater than about 5 and may go as high as 50 (Stoll et al. 1994). The P-wave velocities are nearly unchanged in the mushy layer and close to the velocity of acoustic waves in water; therefore, the dispersion of the Scholte waves is largely controlled by the small S-wave velocity and its vertical variation near the bottom.

The inversion of dispersion curves is in general non-linear and non-unique. Firstly, we aim to derive a simple model with two layers only; the S-wave velocities and interface depths are allowed to vary over a large range during inversion. Information on the P-wave velocities were taken from the experiment report, a P-wave refraction seismic study of Grevemeyer et al. (1999), and

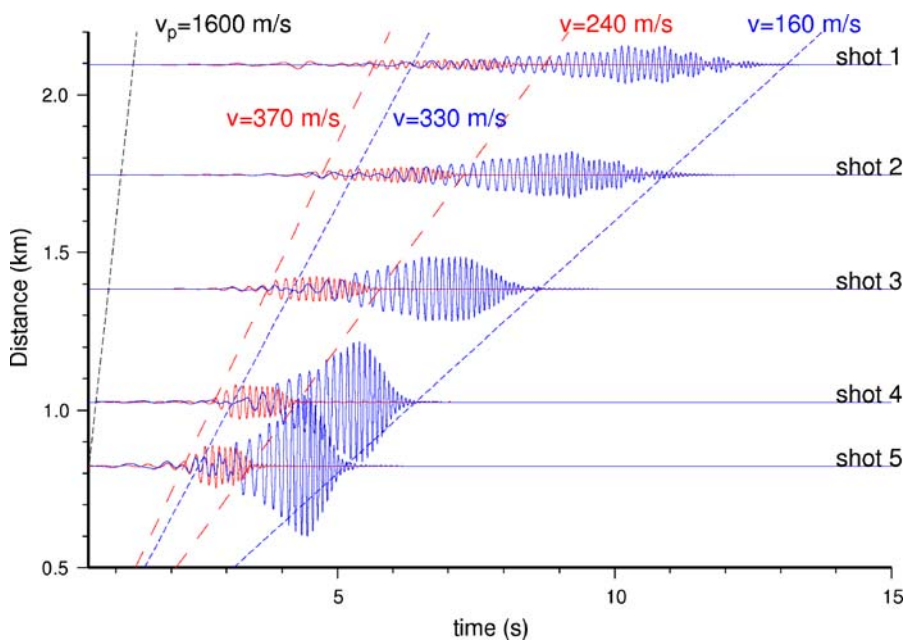

Fig. 6 Record section of the fundamental mode (*blue*) and first higher mode (*red*) Scholte wave after separation by the phase-matched filter approach. See Fig. 2 for further explanations

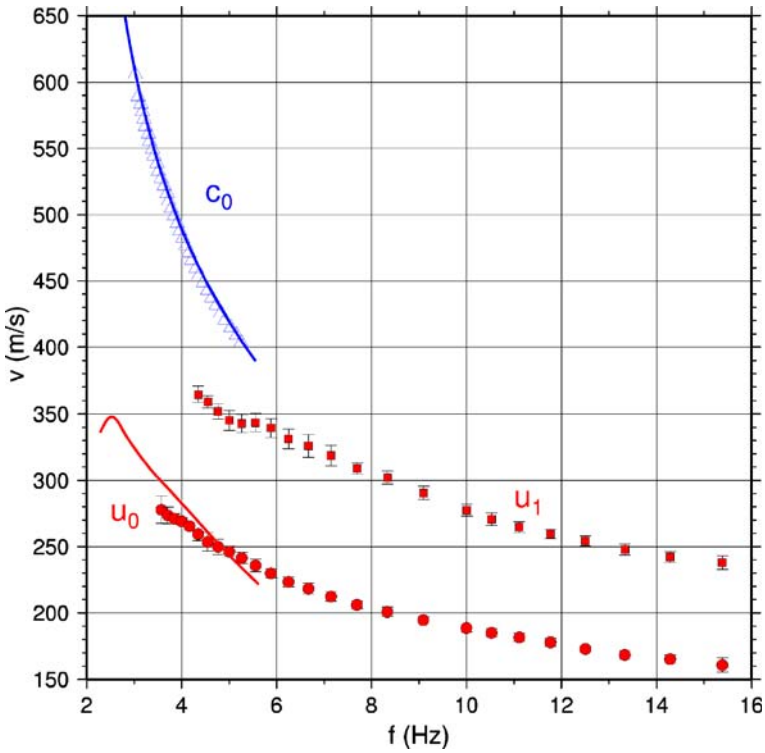

Fig. 7 Group (*u*, *red circles and squares*) and phase velocities (*c*, *blue open triangles*) as finally used for interpretation. Subscript 0 and 1 indicate the fundamental and first higher mode, respectively. Estimated errors are indicated. The phase velocities are interpolated (*blue continuous line*) in order to estimate the corresponding group velocity of the fundamental mode (*red continuous line*)

from borehole 757 ODP results in Peirce et al. (1989a). We apply a direct search algorithm to invert simultaneously group velocities of the fundamental and first higher mode as well as the short branch of phase velocities. Error estimates are considered while calculating misfit values and the inversion result quantify the uncertainties in the model space. A least squares norm is taken as a measure for fit or misfit. The direct search algorithm is based on a neighborhood algorithm and the forward method uses matrix solutions for a stack of homogeneous elastic layers. The method is described in detail by Wathelet et al. (2004) and Wathelet (2008) (see program Dinver from Geopsy package).

The following modeling scheme is selected. The first layer (mushy layer) with the power law increase of shear wave velocity and constant P-wave velocity and density is chosen. Below, we allow one more layer over a half space. No parameter gradients are permitted in this layer and the half space. The density is allowed to vary over a wide range. The variability of the P-wave velocity is more limited according to the independent information available. The Poisson ratio in both layers is varied between 0.2 and 0.5; the ratio in the underlying half space is bounded between 0.22 and 0.3. In other words, the S-wave velocity is allowed to vary over a broad range of parameters. The depth of the interfaces is not fixed. During the last run of the nearest neighborhood inversion, we searched 30,600 different models.

Figure 8 shows the data-fit for the joint inversion, i.e., frequency-dependent group and phase velocities (slowness). Red and yellow colors represent optimal models with smallest misfits. The fundamental and first higher mode group velocities and the phase velocity could be consistently explained with a common model. The fit of the joint inversion is considered as sufficient or good and is within the range of estimated uncertainties over most parts of the dispersion curves. By trial and error inversion, we confirm that the interpretation of the first higher mode is correct, since other associations to even higher modes could not be consistently fitted.

The corresponding depth models are plotted in Fig. 9 with the same color scale as in Fig. 8. Only

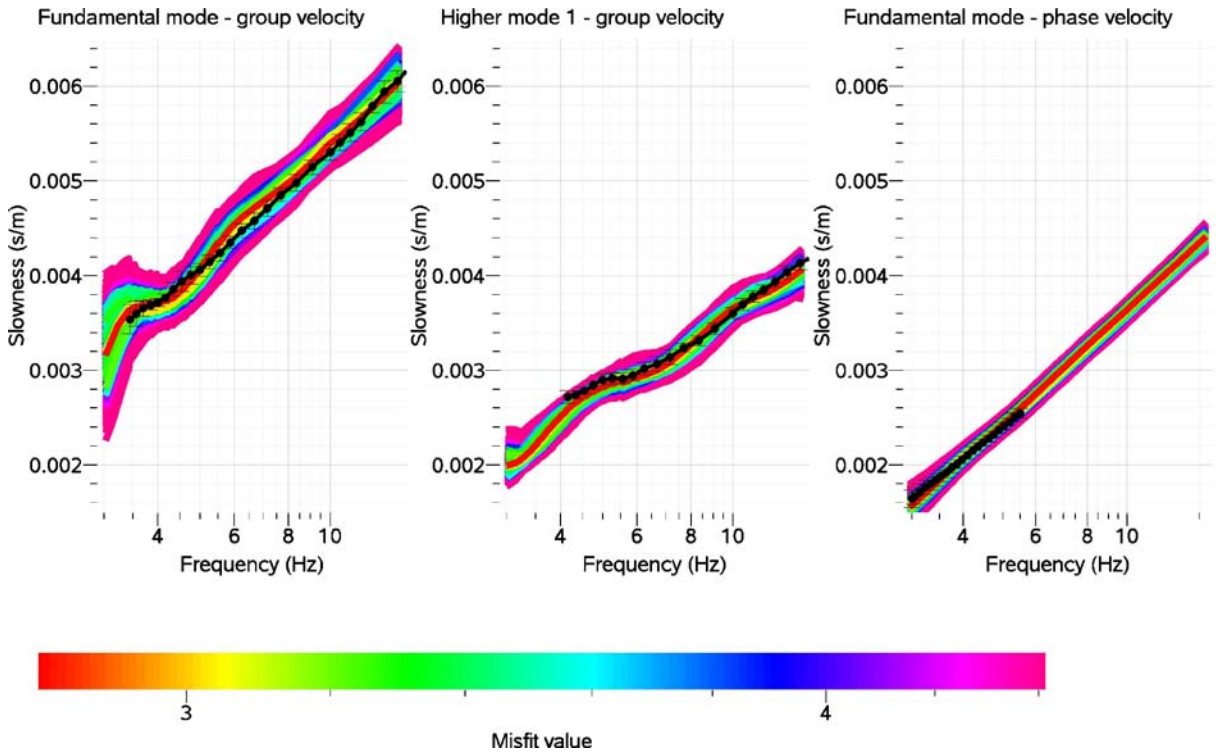

Fig. 8 Inversion results (*colored lines*) are compared to observed group and phase velocities (*black circles*). The figure is slowness versus frequency

depth down to 500 m is plotted since the parameters in deeper levels could not be constrained. The small misfit P-wave velocity models resemble pretty much the velocity model obtained from refraction seismics. A strong velocity increase is observed at about 150 m (2,100 to 2,500 m/s) and at 350 m depth (2,500 to about 3,800 m/s). However, the P-wave velocity is in general badly constrained by the Scholte wave dispersion and should not be over interpreted. The same conclusion is drawn for the density (not plotted in Fig. 9). The S-wave velocities appear well constrained within the uppermost 150 m. They are as low as about 140 m/s at the seafloor and increase quickly to about 600 m/s at a depth of 80 m. This strong velocity gradient is a reliable result. At about 80 m, a velocity increase to about 900 m/s is indicated. The velocity jump at a depth of about 350 m is not very well resolved and S-wave velocities are more closely linked to P-wave velocity in the underlying half space.

The low shear wave velocities in the uppermost meters below the seafloor (bsf) indicate soft unconsolidated sediments (mud). Such a soft uppermost layer was mentioned in the ODP report as nanofossil layer at a depth of 16 m with an S-wave velocity of about 280 m/s. At 148 m depth bsf, the lithological profiles at the ODP site 757 indicate an interface between different volcanic deposits (Peirce et al. 1989a). At about 350 m depth bsf, the lithological profiles at the ODP site 757 indicate an interface between basic igneous and volcanic tuff. A strong jump in P-wave velocity from 2,000 to about 3,500 m/s was found at this depth and interpreted with the top of the basaltic layer (Grevemeyer et al. 1999).

6 Waveform modeling

The inversion of dispersion curves is a kinematics problem and independent of wave amplitudes. Intrinsic attenuation of waves or the relative strength of Airy phases cannot be studied with velocity data alone. Intrinsic attenuation,

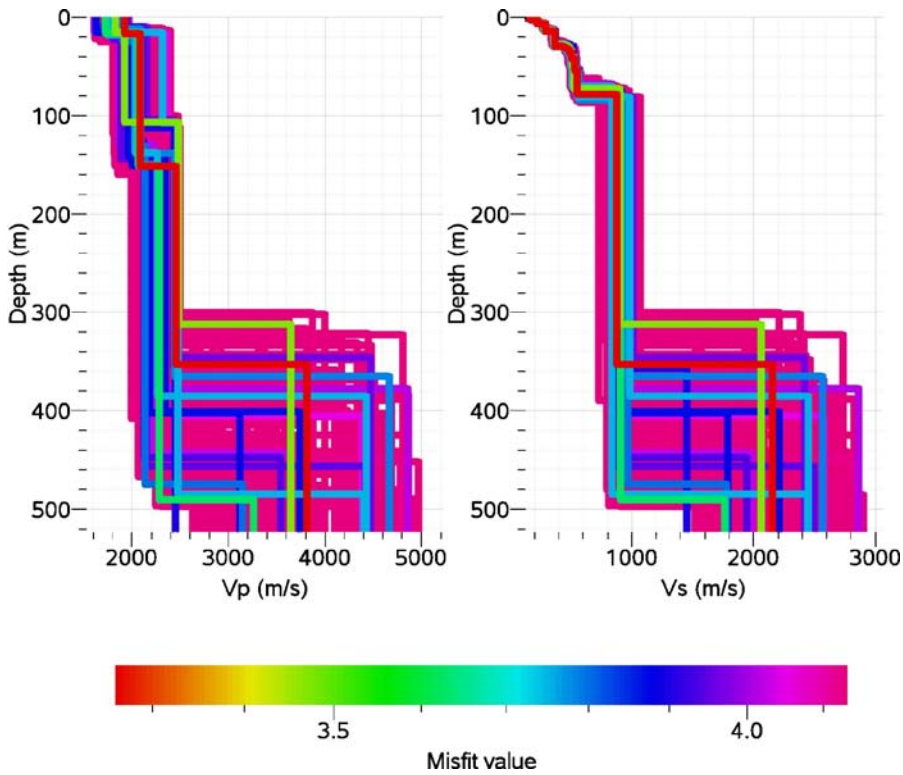

Fig. 9 Inversion results for P- and S-wave velocities. Best fitting models are indicated by *red colors*. The possible parameter range is indicated by the region that is covered by models

however, is possibly strong in the mushy layer and a parameter of interest. We analyze the amplitude pattern of Scholte waves and the intrinsic attenuation by means of a full waveform modeling. A good fit between synthetic and experimental seismograms further provides a reasonable base to verify the inverted velocity models.

We use the reflectivity-based program of Wang (1999) (qseis). Single or general moment tensor point sources can be considered and near- and far-

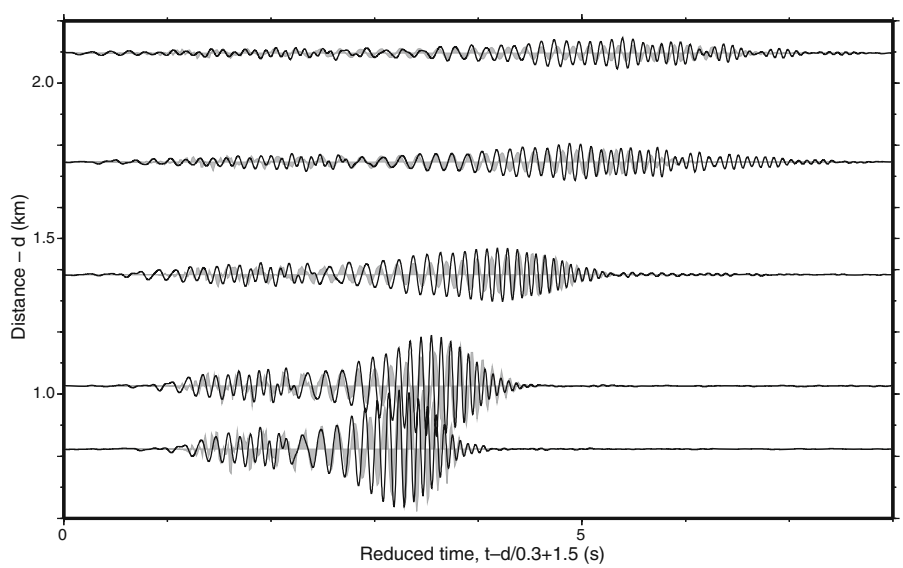

Fig. 10 Waveform modeling results in comparing with experiment data. The *solid lines* are experiment data. *Black filled wiggles* are synthetic data. Data are scaled to a common factor

field body waves, surface waves, and inhomogeneous waves are modeled at the seafloor as well as any possible multiple reflections and diffractions. Due to its completeness, the method is an important contribution to the calculation of synthetic seismograms and is often used for modeling purposes and the inversion of observed seismograms.

We simulate an implosive point source as isotropic moment tensor (explosion source) with negative moment. The source is located at the seafloor. A normalized squared half-sinusoid with the duration of 0.04 s is taken as source time function. The instrument response is considered in the synthetic data which resemble velocity-proportional signals. The sampling frequency is 1024 Hz. The distances from the source to the receivers are the same as the distance obtained by the 1998 experiment. The synthetic seismograms are first computed on the basis of the models obtained from the inversion. The parameters of the layers are then adjusted by trial and error to obtain a better fit between the observed and the synthetic waveforms.

Figure 10 compares the vertical components of the synthetic seismogram and the observation. The main features of the observed wavefield, especially amplitudes and envelopes, could be well modeled. A Qs value for S waves of only 40 is needed for the uppermost layer with a thickness of about 7 m in order to ensure a good fit for all the observed seismograms along the profile. Qs in the layers below could be as high as 1,000. Moreover, the Qp value of P waves was uncritical. Although the amplitudes of the synthetic traces look very similar to the observed ones, the phase pattern of the dispersive waves could not be fitted. It may be explained by the unknown behavior of the source time at high frequencies or due to a frequency-dependent Qs.

The parameters of the reflectivity-based model are shown in Fig. 11. Variations of the P-wave velocities and densities had very little influence on the synthetic waveforms and therefore are not altered, while the S-wave velocity and intrinsic attenuation (Qs) are optimized. The S-wave velocity at the fluid–solid interface is about 195 m/s. A very low Qs value of 40 is required in this mushy layer. It is self-explained by the fact that damping makes a significant impact at the soft seafloor layer which is generally very thin. The S-wave velocity of the mushy layer increases gradually in depth. At the depth of 16 m, the S-wave velocity jumps to a value of 350 m/s. The S-wave velocity has a value of 680 m/s at 150 m bsf. Qs values are kept constant at 1,000 in the layers below the mushy layer. After many tests of different models, we realize that changes in the model within 150 m bsf have main influence on results. It is also indicating again that the frequency ranges available has almost no resolution at larger depths (Figs. 11 and 12).

7 Sensitivity analysis

For evanescent waves such as Scholte–Rayleigh waves and Love waves, long-wavelength waves penetrate deeper into the half space than short-wavelength waves. Sensitivity kernel describes how exactly the structure in a certain depth in-

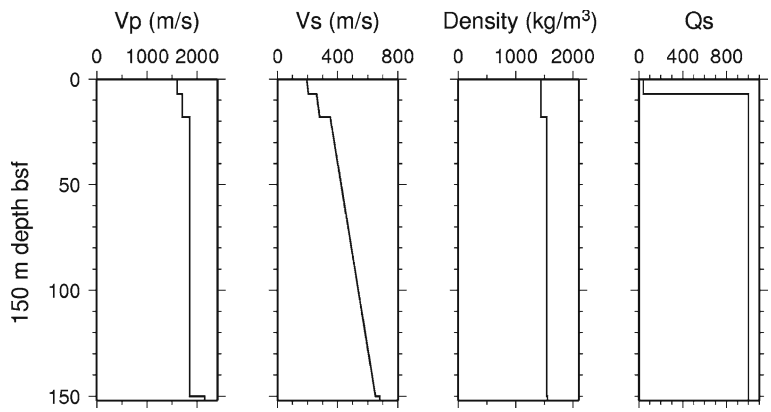

Fig. 11 Seismic parameters derived from waveform modeling. The parameters are displayed for the first 150 m bsf. From the *left*: P-wave velocities (*Vp*) and S-wave velocities (*Vs*), densities of layers and attenuation of S-waves (*Qs*)

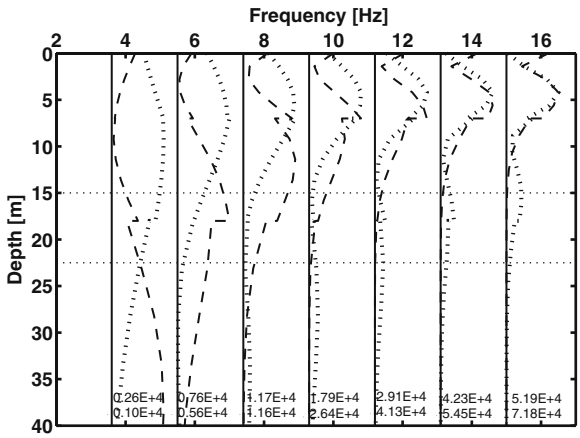

Fig. 12 Sensitivity kernel of the fundamental mode (*dashed*) and first higher mode (*dotted*) with respect to S-wave velocity. The inverted model was used for calculation. Kernels are scaled to a common maximum in each panel. The *numbers inside the panels* indicate the maximum values of the fundamental modes (*bottom*) and the first modes (*top*)

terval influences a wave of a particular frequency. Moreover, sensitivity kernel represents the maximum particle motion at a certain depth as a function of frequency, which can be computed from a reference Earth model.

The general form of 1-D sensitivity kernels for a local shear wave velocity perturbation is given below:

$$\frac{\delta c\,(r_0,\ \omega)}{c} = \int_0^a K_\beta\,(r,\omega)\frac{\delta\beta\,(r_0,r)}{\beta}dr$$

Where:

$K_\beta\,(r,\omega)$ local 1-D sensitivity kernel to shear wave speed and the integration is taken over the Earth's radius R

$\delta\beta$ local shear wave speed perturbations
r_0 unit vector defined on a unit sphere
r variable of Earth radius and varies in the range of 0–R
c_0 reference phase velocity

We present sensitivity kernel analysis of shear wave velocity as a function of depth and frequency. The test which is performed with the use of FLSPHER package (Friederich and Dalkolmo 1995) is aimed to see how well the velocities in different depth intervals are constrained by observed modes.

In Fig. 12, the sensitivities of the fundamental mode (dashed line) and the first higher mode (dotted) are shown in the frequency range between 1 and 18 Hz. The fundamental mode shows maximum sensitivity for high frequencies and shallow depth (0–18 m bsf). High frequency fundamental mode carries information about the vertical gradient at the seafloor. At 4 Hz, the fundamental mode senses layers in 40 m bsf or deeper.

The first higher mode has in general smaller sensitivity which peaks partly in different depth ranges. Both modes carry complementary information and are most sensitive to the depth between 0 and about 30 m bsf.

8 Discussion and conclusion

We have used two methods to analyze Scholte waves and derive the S-wave velocity and Qs structure in the uppermost meters. The measurement of phase dispersion caused problems in our data in correctly identifying the fundamental and first higher mode. However, using additional available information and comparison with theoretical phase velocities were helpful at lower frequencies between 3 and 5 Hz. On the contrary, group velocities could be reliably estimated and were helpful to constrain the velocity structure below the seafloor. The complete waveform modeling was a more time-consuming task but resulted in good fits of amplitudes and insights in the intrinsic attenuation of S waves in the uppermost few meters. The waveform modeling does not rely on mode identification. Other modern approaches, equivalent to full waveform studies, have not been applied to the dataset in this study but are described by Forbriger (2003a, b).

In our study, the thickness and parameters of the uppermost mushy layer was well resolved. The top mushy layer at the experimental site is possibly only about 16 m thick. The intrinsic attenuation of S waves is relatively high with a Qs value of about 40. S-wave velocities are 195 m/s or even smaller in the first few meters bsf. With a P-wave velocity of about 1,600 m/s, the Poisson

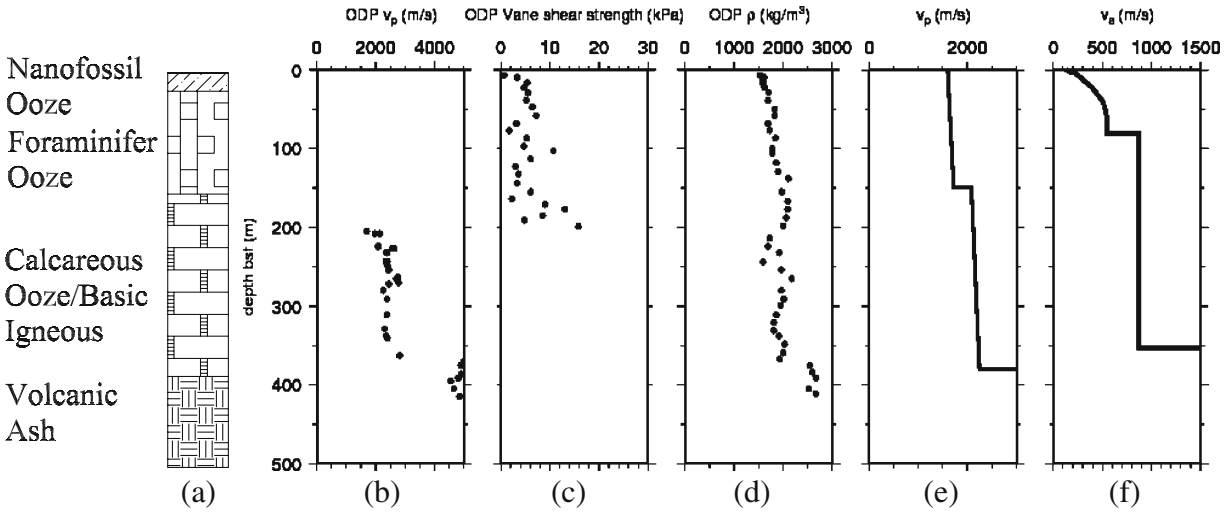

Fig. 13 **a** Lithologic structure about 500 m below seafloor from ODP report, Peirce et al. (1989a). **b**, **c**, **d** P-wave velocity, vane-shear strength. Density obtained from ODP report, Peirce et al. (1989a). **e** P-wave velocity model collected from P-wave study of Grevemeyer et al. (1999). **f** The image of Vs at 500 m bsf, obtained from smallest misfit model of the group velocity inversion

ratio is about 0.49 in the mushy layer. The soft mushy layer is mostly controlling the propagation and dispersion of the Scholte waves between 5 and 10 Hz.

How does our S-wave velocity model compare to measurements from ODP site 757 and P-wave study of Grevemeyer et al. (1999)? Borehole measurements of the P-wave velocity, density, vane-shear strength, and lithology have been described to a depth of 500 m in Fig. 13. Borehole S-wave data was absent from the ODP report (Peirce et al. 1989a).

The uppermost 16 m at the ODP site consist of soft sediments (foraminiferal ooze) with a vane-shear strength increasing from 0 to 6 kPa (Fig. 13). This soft layer is not seen in P-wave data but resolved in our S-wave velocities. The layer thickness in the ODP report is estimated to be about 25 m. Our S-wave velocity profile indicates a strong gradient following a potential increase. A similar trend is indicated in the vane-shear strength of the ODP measurements, although the data show much scattering below about 40 m depth. The ODP site 757 measurements (Fig. 13) find a third layer of basic igneous in a depth of about 370 m. At this layer interface, there is a strong jump in P-wave velocity from 2,000 to about 3,500 m/s. Our S-wave velocity increases in a similar level; however, the resolution of the 3–15 Hz Scholte waves has been small at this depth level. Additionally, there is a strong S-wave discontinuity in between 350 m and about 1.0 km bsf. In summary, the derived velocity model correlates well with borehole data at the ODP site. The mushy layer and the strong gradient in S-wave velocity within the uppermost few meters bsf is resolved by the Scholte wave analysis and for instance hidden in bottom source P-wave studies.

Some other studies derived S-wave velocities in the uppermost 150 m from ocean-bottom-generated Scholte waves. Nolet and Dorman (1996) used waveform fitting to show that starting from 30 m/s, S-wave velocity increases with a gradient of 2.8 m/s per meter over the first 150 m of sediment. Ritzwoller and Levshin (2002) constructed a reliable S-wave model to a depth of 200 m. In other studies, Forbriger (2003a, b) observed a remarkably good resolution of S-wave velocity in 6 and 16 m down to the bedrock, respectively. With their promising approach, Bohlen et al. (2004) are able to apply to a dense net of profiles to derive 2-D models of surface S-wave velocity.

The experiment may be used as a guideline for future seafloor experiments based on Scholte waves and implosion sources. The frequency content of the implosion sources has been documented between 1 and about 15 Hz. Higher frequencies to possibly about 1,000 Hz have been observed in P waves, but our Scholte waves had only been measured between 1 and 15 Hz. Since group velocities are as slow as hundreds of meters per second or less, the recording time has been sufficiently long. The depth sensitivity of such an experiment is smaller than 50 m.

The simultaneous inversion of group velocities and phase velocities has been successful and helpful to interpret different modes correctly. The phase velocity estimates have been difficult because of the aliasing problem, which can only be avoided if stations or shots are placed in close distance of a few tens of meters. Such an experiment design, however, would be difficult to control from the ship.

Acknowledgements The work was funded by SPICE—Seismic wave Propagation and Imaging in Complex media, a European network. The authors are grateful to Robert Herrmann and Rolf Herber for their supports during the preparation of this document. Matthias Ohrnberger helped with the group velocity inversion using the Dinver package, which is greatly acknowledged. Thanks are also expressed to two reviewers for their good suggestions and comments, which improved the paper a lot. Data acquisition was supported by the Bundesminister für Bildung, Wissenschaft, Forschung und Technologie (grant 03G0131A) and by the Deutsche Forschungsgemeinschaft (grant Vi 133/3).

References

Amundsen L, Reitan A (1995) Decomposition of multicomponent seafloor data into up- and downgoing P- and S-waves. Geophysics 60:563–572. doi:10.1190/1.1443794

Bhattacharya SN (1983) Higher order accuracy in multiple filter technique. Bull Seismol Soc Am 73:1395–1406

Bohlen T, Kugler S, Klein GF,Theilen F (2004) 1.5D inversion of lateral variation of Scholte wave dispersion. Geophys 69(2):330–344

Dziewonski A, Bloch S, Landisman M (1969) A technique for analysis of transient seismic signals. Bull Seismol Soc Am 59:427–444

Flueh ER, Reichert C (1998) Cruise report SO131, SINUS—Seismic investigations at the Ninetyeast Ridge Observatory using SONNE and JOIDES Resolution during ODP leg 179, GEOMAR Report, 72

Forbriger T (2003a) Inversion of shallow-seismic wavefields: I—Wavefield transformation. Geophys J Int 153:719–734. doi:10.1046/j.1365-246X.2003.01929.x

Forbriger T (2003b) Inversion of shallow-seismic wavefields: II—Inferring subsurface properties from wavefield transforms. Geophys J Int 153:735–752. doi:10.1046/j.1365-246X.2003.01985.x

Friederich W, Dalkolmo J (1995) Complete synthetic seismograms for a spherically symmetric earth by a numerical computation of the Green's function in the frequency domain. Geophys J Int 122:537–550

Grevemeyer I, Flueh ER, Herber R (1999) Constraint on the shallow seismic structure at Ocean Drilling Program Site 1107, Ninetyeast Ridge, from implosive bottom sources and airgun shots. Geophys Research Letters 26(7):907–910, Apr 1

Herber R, Grevemeyer I, Exner O, Villinger H, Weigel W (1999) Seismo-acoustic implosive source for seismic experiment on the ocean floor. Mar Geophys Res 20:239–247. doi:10.1023/A:1004552406168

Herrin E, Goforth T (1977) Phase-matched filters: application to the study of Rayleigh waves. Bull Seismol Soc Am 67:1259–1275

Herrmann RB, Ammon CJ (2004) Computer programs in seismology, User's Manual V3.30

McMechan G, Yedlin MJ (1981) Analysis of dispersive waves by wave field transformation. Geophysics 46:869–874. doi:10.1190/1.1441225

Müller G (2001) Volume change of seismic sources from moment tensors. Bull Seismol Soc Am 91:880–884. doi:10.1785/0120000261

Nolet G, Dorman LM (1996) Waveform analysis of Scholte modes in ocean sediment layers. Geophys J Int 125:385–396. doi:10.1111/j.1365-246X.1996.tb00006.x

Osen A, Amundsen L, Reitan A (1999) Removal of water-layer multiples from multicomponent sea-bottom data. Geophysics 64:838–851

Parkes G, Hatton L (1986) The marine seismic source. Reidel, Dordrecht

Peirce JW, Weissel JK et al (1989a) Site 757, Proc. ODP, Init. Repts.,121, College Station, TX (Ocean Drilling Program), 305–358 and 517–537

Ritzwoller MH, Levshin AL (2002) Estimating shallow shear velocities with marine multicomponent seismic data. Geophysics 67(6):1991–2004. doi:10.1190/1.1527099

Stoll R, Bryan G, Bautista E (1994) Measuring lateral variability of sediment geoacoustic properties. J Acoust Soc Am 96:427–438

Thorwart M (2006) Wavefield methods to analyze passive ocean bottom seismic data. Application to the Tyrrhenian sea. PhD thesis, Universität Hamburg

Thorwart M, Dahm T (2005) Wavefield decomposition for passive ocean bottom seismological data. Geophys J Int 163:611–621. doi:10.1111/j.1365-246X.2005.02761.x

Wathelet M (2008) An improved neighborhood algorithm: parameter conditions and dynamic scaling. Geophys Res Lett 35:L09301. doi:10.1029/2008GL033256

Wathelet M, Jongmans D, Ohrnberger M (2004) Surface wave inversion using a direct search algorithm and its application to ambient vibration measurements. Near Surf Geophys 2004:211–221

Wang R (1999) A simple orthonormalizing method for stable and efficient computations of Green functions. Bull Seism Soc Am 89:733–741